

Environment-Aware Network-Level Design of Generalized Pinching-Antenna Systems—Part II: Geometry-Aware Case

Yanqing Xu, *Senior Member, IEEE*, Zhiguo Ding, *Fellow, IEEE*, Xiu Yin Zhang, *Fellow, IEEE*, Trung Q. Duong, *Fellow, IEEE*, and Tsung-Hui Chang, *Fellow, IEEE*

arXiv:2602.17032v1 [eess.SP] 19 Feb 2026

Abstract—This two-part paper aims to develop an environment-aware network-level design framework for generalized pinching-antenna systems to overcome the limitations of conventional link-level optimization, which is tightly coupled to instantaneous user geometry and thus sensitive to user mobility and localization errors. Part I investigates the traffic-aware case, where user presence is characterized statistically by a spatial traffic map and deployments are optimized using traffic-aware network-level metrics. Part II complements Part I by developing geometry-aware, blockage-aware network optimization for pinching-antenna systems in obstacle-rich environments. We introduce a grid-level average signal-to-noise (SNR) model with a deterministic LoS visibility indicator and a discrete activation architecture, where the geometry-dependent terms are computed offline in advance. Building on this model, we formulate two network-level activation problems: (i) average-SNR-threshold coverage maximization and (ii) fairness-oriented worst-grid average-SNR maximization. On the algorithmic side, we prove the coverage problem is NP-hard and derive an equivalent mix-integer linear programming reformulation through binary coverage variables and linear SNR linking constraints. To achieve scalability, we further develop a structure-exploiting coordinate-ascent method that updates one waveguide at a time using precomputed per-candidate SNR contributions. For the worst-grid objective, we adopt an epigraph reformulation and leverage the resulting monotone feasibility in the target SNR, enabling an efficient bisection-based solver with low-complexity feasibility checks over the discrete candidate set. Simulations results validate the proposed designs and quantify their gains under different environments and system parameters.

Index Terms—Pinching antenna, environment-aware design, average-SNR-threshold coverage maximization, worst-grid average-SNR maximization.

I. INTRODUCTION

In modern wireless deployments, the key performance question is often not how fast the best link can be, but how well the network serves the whole region. Operators are expected to provide broadly uniform service, avoiding persistent weak-coverage areas and large location-to-location disparities, under

Y. Xu is with the School of Science and Engineering, The Chinese University of Hong Kong, Shenzhen, 518172, China (email: xuyanqing@cuhk.edu.cn).

Z. Ding is with the School of Electrical & Electronic Engineering, Nanyang Technological University, 639798, Singapore (e-mail: zhiguo.ding@ntu.edu.sg).

X. Y. Zhang is with the School of Microelectronics, South China University of Technology, Guangzhou 510000, China, and also with the Pazhou Laboratory, Guangzhou 510330, China (e-mail: eexyz@scut.edu.cn).

T. Q. Duong is with the Faculty of Engineering and Applied Science, Memorial University, St. John's, NL A1C 5S7, Canada and also with the School of Electronics, Electrical Engineering and Computer Science, Queen's University Belfast, Belfast, U.K. (e-mail: tduong@mun.ca).

T.-H. Chang is with the School of Artificial Intelligence, The Chinese University of Hong Kong, Shenzhen, 518172, China (email: changtsunghui@cuhk.edu.cn).

practical constraints such as limited site availability, irregular layouts, and evolving usage patterns. This motivates network-level design approaches that treat performance as a spatial quantity and evaluate service quality over a region rather than at a small set of scheduled user locations [1], [2]. Despite this shift, current network-level planning is still largely built upon fixed-site infrastructures, where base stations (BS) and antenna panels are installed at predetermined locations and the network can mainly adapt through antenna tilt/beam patterns, transmit powers, and scheduling [3]–[8]. While effective in many settings, fixed-site deployments inherently lack spatial agility. Especially, when the environment is irregular (e.g., cluttered indoor spaces, partitioned halls, industrial plants, or dense urban canyons), location-dependent propagation conditions can create persistent weak-coverage regions that are difficult to remedy without costly site densification or infrastructure re-configuration. In such cases, improving link-level performance for served users does not necessarily eliminate coverage holes or enhance the worst-location experience, because the effective radiation points remain unchanged.

In this context, generalized pinching antennas introduce a fundamentally different network-level degree of freedom by enabling reconfigurable radiation points along supporting structures, such as dielectric waveguides, leaky coaxial cables, and other pinching-inspired platforms [9]–[11]. By adjusting where energy is effectively radiated or collected along these structures, the network can shift the transmit/receive locations within the service region in a flexible and lightweight manner. This capability complements classical beam-domain adaptation by providing a new lever in the geometry domain. Instead of only shaping beams from fixed sites, the network can also reshape the physical emission/reception locations to better align with region-wide service objectives. Consequently, generalized pinching antennas open up new opportunities for environment-aware network optimization, enabling deployments that improve region-wide coverage and robustness without relying solely on dense fixed-site installations.

This two-part work aims to develop an environment-aware, network-level design methodology for generalized pinching-antenna systems by capturing two fundamental drivers of spatial performance variability. Specifically, Part I focuses on the traffic-aware setting, where user presence is modeled statistically through a spatial traffic map and network performance is assessed via traffic-aware region-wide metrics. However, traffic heterogeneity is only one side of the story. Even

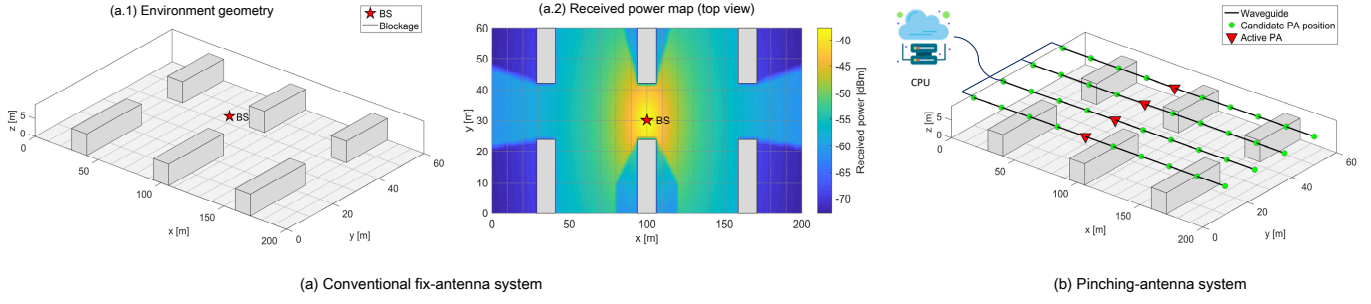


Fig. 1: Illustration of the considered indoor environment and antenna architectures: (a.1) three-dimentional environment geometry with blockages and a fixed BS at the center; (a.2) corresponding top-view received power map for the conventional fixed-antenna system; (b) pinching-antenna system with ceiling waveguides, candidate pinching antenna (PA) positions, and selected active PAs coordinated by a central processing unit (CPU).

with identical demand distributions, service quality can differ sharply across locations due to the propagation environment, which determines where reliable links are feasible in the first place.

In many practical scenarios, such as partitioned indoor spaces, warehouses, shopping malls, and industrial floors—walls, partitions, shelves, and other obstacles create strongly geometry-dependent channel conditions. These structures give rise to line-of-sight (LoS) corridors, abrupt shadow boundaries, and persistent coverage holes that cannot be captured by traffic statistics alone. An example is shown in Fig. 1(a), which shows that the conventional fixed BS cannot guarantee an efficient region-wide coverage. This motivates Part II, which studies geometry-aware network-level generalized pinching-antenna design. Here, “geometry-aware” means that the deployment explicitly incorporates blockage-induced LoS/non-line-of-sight (NLoS) transitions (or LoS feasibility) over the service region based on environment information (e.g., obstacle maps), enabling optimization of region-wide service quality without relying on instantaneous user geometry.

Beyond the numerous studies that focus on LoS-dominated scenarios and demonstrate the benefits of generalized pinching antennas in improving spectral efficiency [12], [13], enhancing energy efficiency [14], [15], and reducing outage probability [16], [17], a growing body of work has begun to investigate blockage-aware modeling and optimization for generalized pinching-antenna systems [18]–[28]. Specifically, a first line of studies adopted probabilistic channel model to characterize LoS blockages and NLoS fading and revealed how blockage reshapes performance trends and design insights. Representative examples include analyzing the impact of LoS blockage on link reliability/outage behavior and developing optimization formulations that explicitly incorporate probabilistic LoS availability into pinching-antenna placement and beamforming for given user sets [18], [20], [21]. Building on these models, a second line of works developed blockage-aware pinching-antenna system designs under diverse service objectives. For instance, blockage-aware pinching-antenna designs were investigated for simultaneous wireless information and power transfer (SWIPT) by jointly optimizing the pinching-antenna position and the power-splitting ratio to maximize the average SNR subject to energy-harvesting constraints [23]. In parallel,

the interplay between blockage-aware modeling and hardware-level effects (e.g., in-waveguide attenuation) was studied in [26], which shown that neglecting in-waveguide attenuation may incur only an insignificant performance loss under typical probabilistic blockage conditions, and proposed a dynamic sample-average-approximation algorithm for stochastic non-convex multi-user designs. Beyond purely statistical blockage models, more recent efforts consider geometry-/map-aware blockage to better reflect obstacle-rich indoor venues. A representative work [27] developed a deterministic cylinder-obstacle blockage model to construct explicit LoS/blocked regions and, based on this geometry-aware model, both discrete and continuous pinching-antenna placement were studied, showing that obstacle-aware spatial reconfigurability can improve performance over fixed-antenna baselines. More recently, leveraging the ability of pinching antennas to reconfigure LoS links, an environment-division multiple access (EDMA) technique was proposed in [28], illustrating the potential of pinching antennas to support multi-user communications through environment-aware spatial adaptation.

However, these studies are still predominantly link-level: they optimize pinching-antenna positions and transceiver parameters for a given user set (often assuming accurate user locations and/or instantaneous channel state information (CSI)) with objectives defined by per-user signal-to-interference-plus-noise ratio (SINR) or data rate. As discussed in Part I, such link-level approaches face several practical limitations. First, since the optimization is tied to instantaneous user geometry, the pinching-antenna positions may need to be recomputed whenever users move or enter/leave the system, resulting in non-negligible control and computational overhead, especially in high-mobility settings. Second, the reliance on accurate user positions makes these designs sensitive to localization errors, which can cause noticeable performance degradation when user locations are imperfect. More fundamentally, optimizing link-level metrics does not necessarily translate into improved network-level service quality over an extended region, particularly in obstacle-rich environments where coverage holes are shaped by blockage geometry.

Motivated by the aforementioned discussions, and without loss of generality, we consider dielectric-waveguide-based pinching antenna as a representative realization in this paper

(Part II) by developing geometry-aware network-level design methodologies for generalized pinching-antenna systems in obstacle-rich environments under an uniform traffic pattern. The main contributions of Part II are summarized as follows:

- **Geometry-aware network-level modeling and metrics:**

We develop a geometry-aware network-level modeling framework for generalized pinching-antenna systems in blockage-rich environments. The service region is discretized into a grid set, and the propagation environment is represented by a collection of three-dimensional cuboid blockages. To capture geometry-induced LoS/NLoS transitions, we introduce a deterministic LoS visibility indicator for each candidate pinching-antenna position and each grid point, which specifies whether the corresponding LoS path is obstructed by any blockage. Under a discrete activation model, we then derive a tractable per-grid average received-SNR expression whose geometry-dependent terms can be precomputed offline once the blockage layout is given. Leveraging these per-grid quantities, we further define a geometry-aware network-level coverage metric and a worst-grid robustness metric, which serve as the basis for the subsequent network-level optimizations.

- **Geometry-aware problem formulation and optimization:**

Building on a blockage-aware, geometry-dependent per-grid average-SNR model, we formulate two network-level design problems: (i) an average-SNR-threshold coverage maximization that selects the activation matrix to maximize the number of grids whose average SNR exceeds a target, and (ii) a fairness-oriented worst-grid average-SNR maximization that improves the minimum average SNR over the service region. We first show that the coverage maximization problem is NP-hard via a polynomial-time reduction from the Maximum Coverage problem, and derive an equivalent mixed-integer linear programming reformulation by introducing binary coverage variables linked through linear SNR constraints. To obtain scalable solutions, we further develop a structure-exploiting coordinate-ascent method that updates one waveguide at a time using precomputable SNR contributions. For the worst-grid objective, we adopt an epigraph reformulation and leverage the resulting monotone feasibility in the target SNR level to enable a bisection-based algorithm, where each feasibility check is implemented efficiently by iteratively updating one waveguide at a time to reduce the total SNR shortfall over all grids.

Extensive simulations validate the proposed geometry-aware designs and quantify their gains. The results show that optimized pinching-antenna activation consistently outperforms fixed-array and random baselines in both average-SNR-threshold coverage and worst-grid average SNR, with clear scaling trends versus the SNR threshold, transmit power, NLoS strength, and the numbers of waveguides/candidates. Top-view SNR maps further illustrate distinct objective-driven behaviors: coverage maximization exploits favorable LoS corridors, whereas worst-grid optimization yields a more balanced activation to mitigate geometry-induced dead zones.

The rest of the paper is organized as follows. Section II

presents the system model, the geometry-aware LoS/NLoS channel model with explicit blockage layouts, and the proposed network-level performance metrics together with their grid-based formulation. Section III formulates the average-SNR-threshold coverage maximization problem and develops a low-complexity coordinate-ascent algorithm. Section IV considers a fairness-oriented worst-grid average-SNR maximization design and proposes a bisection-based algorithm with efficient feasibility checks via coordinate updates. Section V summarizes and compares the traffic-aware and geometry-aware pinching antenna systems and lists several promising future directions. Section VI provides numerical results and performance discussions. Finally, Section VII concludes the paper.

II. SYSTEM MODEL, GEOMETRY-AWARE CHANNEL, AND PERFORMANCE METRICS

In this section, we present the downlink pinching-antenna system with explicit blockages, the geometry-aware channel and signal models for discrete pinching-antenna activation, as well as the network-level performance metrics used for the subsequent optimization.

A. System Model with Blockages and Discrete Candidates

Consider a rectangular communication area of size $D_x \times D_y$, as shown in Fig. 1(b). A CPU coordinates N dielectric waveguides deployed below the ceiling at height d_v , all aligned along the x -axis and uniformly spaced along the y -axis with spacing $d_h = D_y/(N-1)$ satisfying $d_h \gg \lambda$, where λ denotes the carrier wavelength. The index set of waveguides is $\mathcal{N} \triangleq \{1, \dots, N\}$. The feed point position of the n -th waveguide is denoted by $\psi_{0,n} = [0, (n-1)d_h - D_y/2, d_v]^\top, \forall n \in \mathcal{N}$.

In this work, we adopt a discrete pinching-antenna activation model, which serves as a practical counterpart to the continuous positioning model studied in Part I. Specifically, on each waveguide we predefine a finite set of M feasible pinching-antenna locations, and the design problem is to select exactly one active candidate per waveguide to optimize the network-level performance.

Formally, for each waveguide $n \in \mathcal{N}$, we define the candidate index set $\mathcal{M} \triangleq \{1, \dots, M\}$ with x -coordinates $\{\tilde{x}_{n,1}, \dots, \tilde{x}_{n,M}\} \subset [0, D_x]$. The three-dimensional position of candidate $m \in \mathcal{M}$ on waveguide n is given by

$$\psi_{n,m}^{\text{pin}} = [\tilde{x}_{n,m}, (n-1)d_h - D_y/2, d_v]^\top. \quad (1)$$

To indicate which candidate is activated on each waveguide, we introduce binary variables $a_{n,m} \in \{0, 1\}$, where $a_{n,m} = 1$ means that the pinching antenna at $\psi_{n,m}^{\text{pin}}$ is activated and $a_{n,m} = 0$ otherwise. Our design activates exactly one pinching antenna per waveguide, which yields

$$\sum_{m=1}^M a_{n,m} = 1, \quad \forall n \in \mathcal{N}. \quad (2)$$

Collecting $\{a_{n,m}\}$ into a binary activation matrix results in

$$\mathbf{A} \triangleq [a_{n,m}]_{n \in \mathcal{N}, m \in \mathcal{M}} \in \{0, 1\}^{N \times M}, \quad (3)$$

where each row of \mathbf{A} contains exactly one nonzero entry and specifies the active pinching-antenna position on the corresponding waveguide. The matrix \mathbf{A} will serve as the optimization variable in the subsequent geometry-aware design.

As in Part I, we discretize the service region into N_h grids along the x -direction and N_v grids along the y -direction. The grid sizes are written as

$$\Delta_u \triangleq \frac{D_x}{N_h}, \quad \Delta_v \triangleq \frac{D_y}{N_v}. \quad (4)$$

The center of grid (u, v) is given by

$$x_u = \left(u - \frac{1}{2}\right)\Delta_u, \quad y_v = -\frac{D_y}{2} + \left(v - \frac{1}{2}\right)\Delta_v, \quad (5)$$

for $u = 1, \dots, N_h$ and $v = 1, \dots, N_v$. The representative user position in grid (u, v) is given by

$$\psi_{u,v} = [x_u, y_v, 0]^\top, \quad (6)$$

and we denote the set of grid indices by

$$\Omega \triangleq \{1, \dots, N_h\} \times \{1, \dots, N_v\}, \quad |\Omega| = N_h N_v. \quad (7)$$

This discrete-activation model offers two advantages in the considered geometry-aware setting. First, it simplifies control and implementation by allowing each waveguide to be equipped with a finite number of mechanical or electrical tap points, and the BS only needs to select one tap per waveguide. The configuration can thus be encoded by low-rate digital control signals (one index per waveguide), without requiring continuously tunable positions or fine mechanical actuation. Second, it turns continuous antenna placement into a finite selection problem, which enables efficient geometry-aware optimization via precomputable channel and coverage datasets over the grid set Ω , as will be shown in the following subsections.

B. Geometry-Aware Channel Model

Without loss of generality, we consider K rectangular cuboid blockages (e.g., walls or partitions) in the service region. The three-dimensional geometry of blockage $k \in \mathcal{K} \triangleq \{1, \dots, K\}$ is modeled as

$$\mathcal{B}_k = [x_k^{\min}, x_k^{\max}] \times [y_k^{\min}, y_k^{\max}] \times [0, H_{\text{blk}}], \quad (8)$$

where $H_{\text{blk}} < d_v$ denotes the blockage height, $x_k^{\min}, x_k^{\max} \in [0, D_x]$, and $y_k^{\min}, y_k^{\max} \in [-D_y/2, D_y/2]$.

Recall that the service region is discretized into grids indexed by $(u, v) \in \Omega$, with representative location $\psi_{u,v} = [x_u, y_v, 0]^\top$. For grid (u, v) and a pinching-antenna candidate (n, m) , the complex baseband channel coefficient is denoted by $h_{n,m}(\psi_{u,v}) \in \mathbb{C}$. We adopt a geometry-aware LoS/NLoS model, where the LoS component is deterministically determined by the blockage layout.

We introduce a deterministic LoS visibility indicator $\chi_{n,m}(\psi_{u,v}) \in \{0, 1\}$, where $\chi_{n,m}(\psi_{u,v}) = 1$ means that the LoS path between candidate (n, m) and grid (u, v) is not obstructed by any blockage, and $\chi_{n,m}(\psi_{u,v}) = 0$ otherwise. Accordingly, the channel is modeled as

$$h_{n,m}(\psi_{u,v}) = \chi_{n,m}(\psi_{u,v}) h_{n,m}^{\text{LoS}}(\psi_{u,v}) + h_{n,m}^{\text{NLoS}}(\psi_{u,v}), \quad (9)$$

where the term $h_{n,m}^{\text{LoS}}(\psi_{u,v})$ denotes the LoS component when it exists, while $h_{n,m}^{\text{NLoS}}(\psi_{u,v})$ represents the NLoS channel component [29].

Following the channel model in [10], [30], the LoS component can be written as

$$h_{n,m}^{\text{LoS}}(\psi_{u,v}) = \sqrt{\eta} \frac{\exp\left(-j\frac{2\pi}{\lambda} r_{n,m}(\psi_{u,v}) + j\frac{2\pi}{\lambda_g} \tilde{x}_{n,m}\right)}{r_{n,m}(\psi_{u,v})}, \quad (10)$$

where λ is the carrier wavelength, λ_g is the guided wavelength, and $\eta = c^2/(4\pi f_c)^2$ with c the speed of light and f_c the carrier frequency. Moreover, $r_{n,m}(\psi_{u,v}) \triangleq \sqrt{(x_u - \tilde{x}_{n,m})^2 + C_{n,v}}$ denotes the distance between grid (u, v) with $C_{n,v} \triangleq (y_v - ((n-1)d_h - D_y/2))^2 + d_v^2$.

The NLoS component $h_{n,m}^{\text{NLoS}}(\psi_{u,v})$ captures the aggregate contribution of scattered multipath. We adopt a Rayleigh fading model in which the NLoS term is the superposition of N_c independent scattering clusters

$$h_{n,m}^{\text{NLoS}}(\psi_{u,v}) = \sum_{\ell=1}^{N_c} g_{n,m,\ell}(\psi_{u,v}), \quad (11)$$

where $g_{n,m,\ell}(\psi_{u,v})$ denotes the small-scale fading coefficient associated with the ℓ -th cluster. We model it as

$$g_{n,m,\ell}(\psi_{u,v}) \sim \mathcal{CN}\left(0, \frac{\mu_\ell^2}{r_{n,m}^2(\psi_{u,v})}\right), \quad (12)$$

so that each cluster has zero mean and a distance-dependent average power, where μ_ℓ^2 is the average power of cluster ℓ .

C. Signal Model

Given an activation matrix \mathbf{A} , the effective channel from waveguide n to grid (u, v) is given by

$$\tilde{h}_n(\psi_{u,v}; \mathbf{A}) \triangleq \sum_{m=1}^M a_{n,m} h_{n,m}(\psi_{u,v}), \quad \forall n \in \mathcal{N}, \quad (u, v) \in \Omega, \quad (13)$$

which is essentially the channel coefficient of the activated candidate on waveguide n due to $\sum_{m=1}^M a_{n,m} = 1$. Stacking all waveguides, we define the effective channel vector as

$$\tilde{\mathbf{h}}(\psi_{u,v}; \mathbf{A}) \triangleq [\tilde{h}_1(\psi_{u,v}; \mathbf{A}), \dots, \tilde{h}_N(\psi_{u,v}; \mathbf{A})]^\top \in \mathbb{C}^N. \quad (14)$$

Let s denote the downlink data symbol, satisfying $\mathbb{E}[|s|^2] = 1$. The received baseband signal at grid (u, v) is given by

$$y(\psi_{u,v}) = \sqrt{P} \tilde{\mathbf{h}}^\top(\psi_{u,v}; \mathbf{A}) \mathbf{w}(\psi_{u,v}; \mathbf{A}) s + z_{u,v}, \quad (15)$$

where P denotes the total transmit power, $\mathbf{w}(\psi_{u,v}; \mathbf{A}) \in \mathbb{C}^N$ denotes the downlink beamformer, and $z_{u,v} \sim \mathcal{CN}(0, \sigma^2)$ denotes the received additive white Gaussian noise with σ^2 representing the noise power.

Similar to Part I, the BS employs maximum-ratio transmission (MRT) beamformer based on the effective channel $\tilde{\mathbf{h}}(\psi_{u,v}; \mathbf{A})$, i.e.,

$$\mathbf{w}(\psi_{u,v}; \mathbf{A}) \triangleq \frac{\tilde{\mathbf{h}}^*(\psi_{u,v}; \mathbf{A})}{\|\tilde{\mathbf{h}}(\psi_{u,v}; \mathbf{A})\|}, \quad \|\mathbf{w}(\psi_{u,v}; \mathbf{A})\|^2 = 1, \quad (16)$$

where $(\cdot)^*$ denotes complex conjugation. Under MRT, the instantaneous received SNR at grid (u, v) becomes

$$\begin{aligned} \Gamma(\psi_{u,v}; \mathbf{A}) &\triangleq \frac{P \left| \tilde{\mathbf{h}}^\top(\psi_{u,v}; \mathbf{A}) \mathbf{w}(\psi_{u,v}; \mathbf{A}) \right|^2}{\sigma^2} \\ &= \rho \left\| \tilde{\mathbf{h}}(\psi_{u,v}; \mathbf{A}) \right\|^2, \end{aligned} \quad (17)$$

where $\rho \triangleq P/\sigma^2$.

D. Per-Grid Average Received SNR

Under the blockage-aware channel model, the received SNR varies due to small-scale fading (mainly through the NLoS component). We therefore adopt an average-SNR-threshold performance metric. For the per-grid average received SNR, we have the following lemma

Lemma 1. *Given an activation matrix \mathbf{A} , for grid $(u, v) \in \Omega$, the per-grid average received SNR is given by*

$$\bar{\Gamma}(\psi_{u,v}; \mathbf{A}) = \rho \sum_{n=1}^N \sum_{m=1}^M a_{n,m} \frac{\chi_{n,m}(\psi_{u,v}) \eta + \mu^2}{r_{n,m}^2(\psi_{u,v})}. \quad (18)$$

Proof: See Appendix A. \blacksquare

Lemma 1 shows that, for each grid (u, v) , the average SNR under activation \mathbf{A} depends on $\{a_{n,m}\}$ only through a weighted sum. The weights are entirely determined by the environment geometry (via $\chi_{n,m}(\psi_{u,v})$ and $r_{n,m}(\psi_{u,v})$) and the channel parameters (η, μ^2) . Consequently, once the blockage layout and the grid are fixed, the terms $(\chi_{n,m}(\psi_{u,v}) \eta + \mu^2)/r_{n,m}^2(\psi_{u,v})$ can be precomputed offline for all $(u, v) \in \Omega$, $n \in \mathcal{N}$, and $m \in \mathcal{M}$. These precomputed SNR maps will be used in the following sections to construct geometry-aware coverage metrics and formulate the corresponding network optimization problems.

We emphasize that the linear dependence on \mathbf{A} in (18) stems from the discrete-activation model, where each waveguide selects exactly one candidate from a finite set. This structure supports an offline-online workflow. In particular, once the environment is specified, the geometry-dependent channel/SNR terms can be precomputed offline, and the online design reduces to selecting the activation matrix $\mathbf{A} \in \{0, 1\}^{N \times M}$. In what follows, we build on (18) to formulate geometry-aware pinching-antenna activation optimization problems that choose \mathbf{A} to best match the blockage layout and the desired coverage objectives over the grid set Ω . In particular, we focus on average-SNR-threshold coverage maximization and worst-grid average-SNR maximization.

III. AVERAGE-SNR-THRESHOLD COVERAGE MAXIMIZATION

In this section, we study a coverage-oriented pinching-antenna activation design for the geometry-aware scenario. The key idea is to map the per-grid average SNR in (18) to a binary notion of coverage via an SNR target, and then select the activation matrix \mathbf{A} to maximize the resulting covered area over the grid set Ω . To this end, we first introduce the following definition.

Definition 1 (SNR-threshold coverage). *Given an SNR threshold $\gamma_{\text{th}} > 0$, grid (u, v) is said to be covered under activation \mathbf{A} if its average received SNR satisfies $\bar{\Gamma}(\psi_{u,v}; \mathbf{A}) \geq \gamma_{\text{th}}$. Accordingly, we define the binary coverage indicator as*

$$c_{u,v}(\mathbf{A}) \triangleq \mathbb{1}\{\bar{\Gamma}(\psi_{u,v}; \mathbf{A}) \geq \gamma_{\text{th}}\}, \quad (u, v) \in \Omega, \quad (19)$$

where $\mathbb{1}\{\cdot\}$ denotes the indicator function.

With the above definition, we can now quantify the covered area over the grid set Ω by counting the number of covered grids. Accordingly, the average-SNR-threshold coverage maximization problem is formulated as

$$\max_{\mathbf{A}} \sum_{(u,v) \in \Omega} c_{u,v}(\mathbf{A}) \quad (20a)$$

$$\text{s.t. } \sum_{m=1}^M a_{n,m} = 1, \quad \forall n \in \mathcal{N}, \quad (20b)$$

$$a_{n,m} \in \{0, 1\}, \quad \forall n \in \mathcal{N}, \quad m \in \mathcal{M}. \quad (20c)$$

Here, the objective maximizes the total number of grids whose average received SNR exceeds the target γ_{th} , while the constraints enforce the one-hot activation of a single candidate on each waveguide.

A. Solving the Coverage Maximization Problem

It is challenging to solve the Problem (20) because the objective involves the discontinuous indicator $c_{u,v}(\mathbf{A})$. Fortunately, thanks to the linear form of $\bar{\Gamma}(\psi_{u,v}; \mathbf{A})$ in (18) and the one-hot activation constraints, the problem admits a clean mixed-integer linear programming (MILP) reformulation, as well as a scalable structure-exploiting algorithm.

1) *Exact MILP reformulation:* To handle the discontinuous coverage indicator, we introduce auxiliary binary variables $\{c_{u,v} \in \{0, 1\}\}_{(u,v) \in \Omega}$, where $c_{u,v} = 1$ indicates that grid (u, v) is covered. The coverage condition $\bar{\Gamma}(\psi_{u,v}; \mathbf{A}) \geq \gamma_{\text{th}}$ can be linked to $c_{u,v}$ through the implication

$$c_{u,v} = 1 \Rightarrow \bar{\Gamma}(\psi_{u,v}; \mathbf{A}) \geq \gamma_{\text{th}},$$

which is enforced by the linear constraint

$$\bar{\Gamma}(\psi_{u,v}; \mathbf{A}) \geq \gamma_{\text{th}} c_{u,v}, \quad \forall (u, v) \in \Omega. \quad (21)$$

Importantly, since $\bar{\Gamma}(\psi_{u,v}; \mathbf{A}) \geq 0$, (21) does not require any big- M constant. The following lemma shows that the resulting formulation is equivalent to the original coverage-count objective.

Lemma 2. *For any fixed activation matrix \mathbf{A} , an optimal choice of $\{c_{u,v}\}$ under (21) is given by*

$$c_{u,v}^* = \mathbb{1}\{\bar{\Gamma}(\psi_{u,v}; \mathbf{A}) \geq \gamma_{\text{th}}\}, \quad \forall (u, v) \in \Omega. \quad (22)$$

Consequently, maximizing $\sum_{(u,v) \in \Omega} c_{u,v}$ subject to (21) is equivalent to maximizing the covered-grid count $\sum_{(u,v) \in \Omega} \mathbb{1}\{\bar{\Gamma}(\psi_{u,v}; \mathbf{A}) \geq \gamma_{\text{th}}\}$.

With the introduced auxiliary variables $\{c_{u,v}\}$ and the linear linking constraints (21), Problem (20) is equivalently reformulated as the following MILP

$$\max_{\mathbf{A}, \{c_{u,v}\}} \sum_{(u,v) \in \Omega} c_{u,v} \quad (23a)$$

$$\text{s.t. } \bar{\Gamma}(\psi_{u,v}; \mathbf{A}) \geq \gamma_{\text{th}} c_{u,v}, \forall (u, v) \in \Omega, \quad (23\text{b})$$

$$\sum_{m=1}^M a_{n,m} = 1, \forall n \in \mathcal{N}, \quad (23\text{c})$$

$$a_{n,m} \in \{0, 1\}, \forall n \in \mathcal{N}, m \in \mathcal{M}, \quad (23\text{d})$$

$$c_{u,v} \in \{0, 1\}, \forall (u, v) \in \Omega, \quad (23\text{e})$$

Compared with the original formulation (20), the MILP reformulation (23) removes the discontinuous indicator function from the objective by introducing auxiliary binary coverage variables and linear linking constraints. As a result, (23) becomes a standard mixed-integer linear program that can be solved by off-the-shelf MILP solvers when the grid size $|\Omega|$ and the candidate count M are moderate. Nevertheless, as stated in Proposition 1, problem (23) is still NP-hard in general and may incur prohibitive complexity when $|\Omega|$ and/or M is large.

Proposition 1. *Problem (23) is NP-hard.*

Proof: See Appendix B. \blacksquare

Despite the NP-hardness of (23), in the following we devise a low-complexity algorithm to obtain high-quality solutions with scalable computational cost.

2) A structure-exploiting coordinate-ascent algorithm:

While Problem (23) can be solved by off-the-shelf MILP solvers (e.g., via branch-and-bound) for moderate problem sizes, its computational burden may become prohibitive when the grid set Ω is dense or the number of candidates M is large [31]. We therefore develop a low-complexity algorithm that exploits two key structures: (i) the one-hot constraint $\sum_{m=1}^M a_{n,m} = 1$ for each waveguide n , and (ii) the additive form of the per-grid average SNR in (18).

Given an activation matrix \mathbf{A} , let m_n denote the currently activated candidate on waveguide n , i.e., $a_{n,m_n} = 1$. For each grid (u, v) , define the average SNR excluding waveguide n as

$$\bar{\Gamma}_{-n}(\psi_{u,v}; \mathbf{A}) \triangleq \bar{\Gamma}(\psi_{u,v}; \mathbf{A}) - \rho \bar{G}_{n,m_n}(\psi_{u,v}), (u, v) \in \Omega. \quad (24)$$

If waveguide n switches to candidate m , the resulting average SNR at grid (u, v) becomes

$$\begin{aligned} \bar{\Gamma}(\psi_{u,v}; \mathbf{A}_{n \rightarrow m}) &= \bar{\Gamma}_{-n}(\psi_{u,v}; \mathbf{A}) \\ &\quad + \rho \bar{G}_{n,m}(\psi_{u,v}), (u, v) \in \Omega, \end{aligned} \quad (25)$$

where $\mathbf{A}_{n \rightarrow m}$ denotes the activation matrix obtained by replacing row n of \mathbf{A} with $a_{n,m} = 1$.

Therefore, when updating waveguide n , we can enumerate $m \in \mathcal{M}$ and select the candidate that yields the largest number of covered grids

$$m_n^* \in \arg \max_{m \in \mathcal{M}} \sum_{(u,v) \in \Omega} \mathbb{1}\{\bar{\Gamma}_{-n}(\psi_{u,v}; \mathbf{A}) + \rho \bar{G}_{n,m}(\psi_{u,v}) \geq \gamma_{\text{th}}\}. \quad (26)$$

To improve stability, when multiple candidates achieve the same covered-grid count, we use the following tie-breaker: choose the candidate that maximizes the total SNR margin above the threshold,

$$\sum_{(u,v) \in \Omega} \left[\bar{\Gamma}_{-n}(\psi_{u,v}; \mathbf{A}) + \rho \bar{G}_{n,m}(\psi_{u,v}) - \gamma_{\text{th}} \right]^+, \quad (27)$$

where $[x]^+ \triangleq \max\{x, 0\}$.

Starting from any feasible $\mathbf{A}^{(0)}$, we iterate over $n = 1, \dots, N$ and update one waveguide at a time using (26) (until no further improvement is observed). Each update optimizes the coverage objective over the finite candidate set of the current waveguide while fixing all other waveguides, and hence the covered-grid count is nondecreasing across iterations. Since the feasible set is finite, the algorithm terminates after a finite number of iterations.

Each waveguide update evaluates M candidates over $|\Omega|$ grids, leading to a per-iteration complexity of $\mathcal{O}(NM|\Omega|)$. Since the quantities $\{\bar{G}_{n,m}(\psi_{u,v})\}$ are precomputable offline, the online computation consists of simple additions and threshold comparisons.

IV. WORST-GRID AVERAGE-SNR MAXIMIZATION

In this section, we consider a fairness-oriented design objective. Specifically, we seek to enhance the weakest grid in the service region by maximizing the minimum per-grid average received SNR over Ω . This criterion is particularly relevant in blockage-aware environments, where some grids may otherwise experience persistently low SNR due to unfavorable LoS visibility.

A. Problem Formulation

Recall that $\bar{\Gamma}(\psi_{u,v}; \mathbf{A})$ denotes the average received SNR at grid (u, v) under activation \mathbf{A} . The worst-grid average-SNR maximization problem can be formulated as

$$\max_{\mathbf{A}} \min_{(u,v) \in \Omega} \bar{\Gamma}(\psi_{u,v}; \mathbf{A}) \quad (28\text{a})$$

$$\text{s.t. } \sum_{m=1}^M a_{n,m} = 1, \forall n \in \mathcal{N}, \quad (28\text{b})$$

$$a_{n,m} \in \{0, 1\}, \forall n \in \mathcal{N}, m \in \mathcal{M}. \quad (28\text{c})$$

To obtain an equivalent mixed-integer linear formulation, we introduce an auxiliary variable t representing the worst-grid average SNR. Then, problem (28) can be equivalently rewritten in epigraph form as

$$\max_{\mathbf{A}, t} t \quad (29\text{a})$$

$$\text{s.t. } \bar{\Gamma}(\psi_{u,v}; \mathbf{A}) \geq t, \quad \forall (u, v) \in \Omega, \quad (29\text{b})$$

$$\sum_{m=1}^M a_{n,m} = 1, \forall n \in \mathcal{N}, \quad (29\text{c})$$

$$a_{n,m} \in \{0, 1\}, \forall n \in \mathcal{N}, m \in \mathcal{M}. \quad (29\text{d})$$

Although (29) removes the inner minimization operator, it remains challenging because it is an MILP involving binary variables \mathbf{A} and a continuous SNR variable t . To develop a structured solution, we next exploit a monotonic feasibility property with respect to the target average SNR level.

B. Monotonic Feasibility in the Target SNR Level

For a given target $t \geq 0$, consider the following feasibility question: *Is there an activation matrix \mathbf{A} such that*

$\bar{\Gamma}(\psi_{u,v}; \mathbf{A}) \geq t$ holds for all $(u, v) \in \Omega$? This feasibility question is monotone in t , as stated below.

Lemma 3. *Given t , the feasible set is defined as*

$$\mathcal{F}(t) \triangleq \left\{ \mathbf{A} \in \{0, 1\}^{N \times M} \mid \bar{\Gamma}(\psi_{u,v}; \mathbf{A}) \geq t, \forall (u, v) \in \Omega, \sum_{m=1}^M a_{n,m} = 1, \forall n \in \mathcal{N} \right\}. \quad (30)$$

For any $0 \leq t_1 \leq t_2$, we have $\mathcal{F}(t_2) \subseteq \mathcal{F}(t_1)$. Equivalently, if the constraints are feasible at t_2 , then they are also feasible at any $t_1 \in [0, t_2]$.

Proof: Let $0 \leq t_1 \leq t_2$ and take any $\mathbf{A} \in \mathcal{F}(t_2)$. Then $\bar{\Gamma}(\psi_{u,v}; \mathbf{A}) \geq t_2$ for all $(u, v) \in \Omega$, and the one-hot constraints $\sum_{m=1}^M a_{n,m} = 1$ hold for all $n \in \mathcal{N}$. Since $t_1 \leq t_2$, it follows that $\bar{\Gamma}(\psi_{u,v}; \mathbf{A}) \geq t_1$ for all $(u, v) \in \Omega$, while the one-hot constraints remain unchanged. Hence $\mathbf{A} \in \mathcal{F}(t_1)$, which proves $\mathcal{F}(t_2) \subseteq \mathcal{F}(t_1)$. \blacksquare

Lemma 3 shows that the feasibility of the per-grid constraints $\bar{\Gamma}(\psi_{u,v}; \mathbf{A}) \geq t$ is monotone in t : whenever a target level t is achievable, any smaller level is also achievable. This monotonic structure implies that the set of achievable worst-grid SNR levels forms an interval and naturally motivates applying a bisection search over t to solve Problem (29).

C. Bisection-Based Algorithm for Solving Problem (29)

Motivated by the monotonic feasibility property in Lemma 3, we solve Problem (29) via a bisection search on the epigraph variable t . Specifically, we initialize $t_{\min} = 0$ and choose any valid upper bound t_{\max} .¹ At each iteration, we set $t \leftarrow (t_{\min} + t_{\max})/2$ and perform a feasibility check at level t . If the check is successful, we update $t_{\min} \leftarrow t$ and store the corresponding activation matrix; otherwise, we update $t_{\max} \leftarrow t$. The procedure terminates once $t_{\max} - t_{\min}$ is below a prescribed tolerance.

1) Feasibility Check at a Given SNR Level t : For a fixed test value t , the feasibility check amounts to finding an activation matrix \mathbf{A} such that the per-grid average SNR constraints are satisfied:

$$\begin{aligned} \text{find } & \mathbf{A} \\ \text{s.t. } & \bar{\Gamma}(\psi_{u,v}; \mathbf{A}) \geq t, \quad \forall (u, v) \in \Omega, \\ & \sum_{m=1}^M a_{n,m} = 1, \quad \forall n \in \mathcal{N}, \\ & a_{n,m} \in \{0, 1\}, \quad \forall n \in \mathcal{N}, m \in \mathcal{M}. \end{aligned} \quad (31)$$

If (31) is feasible, then the target level t is achievable; otherwise, it is not. Problem (31) is a 0–1 linear feasibility problem and can be handled by a MIP solver. However, when $|\Omega|$ is large or M is large, repeatedly calling a MIP solver within bisection may incur a high computational cost. We therefore develop a low-complexity feasibility check based on coordinate updates.

¹In practice, t_{\max} can be set conservatively using a relaxed bound or an empirical upper bound obtained from the precomputed channel/SNR maps.

2) Low-Complexity Feasibility Check via Deficit Reduction: For a fixed level t and a current one-hot activation matrix \mathbf{A} , define the per-grid SNR deficit

$$d_{u,v}(\mathbf{A}; t) \triangleq \left[t - \bar{\Gamma}(\psi_{u,v}; \mathbf{A}) \right]^+, \quad (u, v) \in \Omega, \quad (32)$$

and the total deficit

$$D(\mathbf{A}; t) \triangleq \sum_{(u, v) \in \Omega} d_{u,v}(\mathbf{A}; t). \quad (33)$$

Clearly, $D(\mathbf{A}; t) = 0$ implies that \mathbf{A} satisfies $\bar{\Gamma}(\psi_{u,v}; \mathbf{A}) \geq t$ for all $(u, v) \in \Omega$.

Starting from an initial one-hot \mathbf{A} , we sweep over waveguides $n = 1, \dots, N$ and update one waveguide at a time to reduce $D(\mathbf{A}; t)$. Let m_n denote the currently activated candidate on waveguide n (i.e., $a_{n,m_n} = 1$). As in (24), define

$$\bar{\Gamma}_{-n}(\psi_{u,v}; \mathbf{A}) \triangleq \bar{\Gamma}(\psi_{u,v}; \mathbf{A}) - \rho \bar{G}_{n,m_n}(\psi_{u,v}), \quad (u, v) \in \Omega. \quad (34)$$

If waveguide n switches to candidate m , the resulting per-grid average SNR is given by (25), i.e., $\bar{\Gamma}(\psi_{u,v}; \mathbf{A}_{n \rightarrow m}) = \bar{\Gamma}_{-n}(\psi_{u,v}; \mathbf{A}) + \rho \bar{G}_{n,m}(\psi_{u,v})$. We then choose the candidate that minimizes the updated total deficit:

$$m_n^* \in \arg \min_{m \in \mathcal{M}} \sum_{(u, v) \in \Omega} \left[t - \bar{\Gamma}(\psi_{u,v}; \mathbf{A}_{n \rightarrow m}) \right]^+. \quad (35)$$

After several sweeps (or once $D(\mathbf{A}; t)$ no longer decreases), the feasibility check is declared successful if $D(\mathbf{A}; t) = 0$ and unsuccessful otherwise. Combined with the bisection framework above, this yields a low-complexity bisection-based algorithm for worst-grid average-SNR maximization. Notably, each feasibility check involves only simple per-waveguide candidate updates and evaluations of $D(\mathbf{A}; t)$ using the precomputed SNR maps, leading to a low-complexity implementation.

V. SUMMARY AND OUTLOOK

Our two-part papers develop environment-aware design methodologies for pinching-antenna systems from two complementary perspectives. In Part I, we consider a traffic-aware setting where user demand is modeled by a spatial traffic distribution and the propagation environment is captured through a distance-dependent stochastic LoS/NLoS model. Under this setting, we design continuous pinching-antenna positions along the waveguides to optimize traffic-aware network performance metrics. In Part II, we shift to a geometry-aware setting with explicit blockage layouts, where the LoS visibility is deterministically determined by obstacles and each waveguide admits a finite set of candidate pinching-antenna locations. This leads to a practical discrete-activation formulation, for which we develop geometry-aware coverage and fairness optimization strategies based on offline-precomputable SNR maps. Table I summarizes the two baseline settings and highlights how their distinct environment models and control capabilities lead to different performance objectives and algorithmic solutions, together providing a modular foundation for more sophisticated pinching-antenna system designs.

TABLE I: Summary and comparison between Part I and Part II .

Aspect	Part I: Traffic-aware case	Part II: Geometry-aware case
Environment model	Known traffic distribution modeled by a Gaussian-hotspot mixture; propagation follows a distance-dependent stochastic LoS/NLoS model (without explicit obstacles).	Known blockage layout modeled by rectangular cuboids; LoS visibility is deterministically determined by geometry, while NLoS follows distance-dependent random fading.
Service region model	Grid-based service region to enable network-level performance evaluation/optimization.	Grid-based model to enable geometry-aware coverage optimization and offline map construction.
Antenna control model	Pinching antennas can move continuously along each waveguide; locations are real-valued design variables.	Each waveguide has M predefined candidate tap points; antenna activation is controlled via binary variables.
Performance metrics	(i) Traffic-weighted network average SNR; (ii) traffic-restricted worst-grid average SNR over an active set Ω_{act} .	(i) Average-SNR-threshold coverage over Ω ; (ii) worst-grid average SNR over Ω .
Design objectives	Continuous placement to optimize traffic-aware network average SNR and traffic-restricted worst-grid average-SNR.	Discrete activation to optimize average-SNR-threshold coverage and worst-grid average-SNR.
Workflow and solver	Online continuous optimization: candidate-based <i>global maximization</i> for the traffic-weighted average SNR maximization, and BCD with nested bisection for the traffic-restricted worst-grid SNR maximization.	Offline–online discrete optimization: offline SNR-map construction, followed by MILP/coordinate-ascent for coverage maximization and epigraph-based bisection with low-complexity feasibility checks for worst-grid SNR optimization.

TABLE II: Default simulation parameters.

Parameter	Value
Carrier frequency (f_c)	28 GHz
Communication-region size ($D_x \times D_y$)	$200 \times 60 \text{ m}^2$
Waveguide height (d_v)	10 m
Transmit power (P)	40 dBm
Noise power (σ^2)	-70 dBm
NLoS power (μ^2)	-60 dBm
Number of PAs / waveguides (N)	4
Number of grids ($N_h \times N_v$)	400×120
Algorithm tolerance (ϵ_t, ϵ_d)	10^{-3}
Obstacle height (H_{blk})	6 m

Overall, this work establishes two basic environment-aware baselines for pinching-antenna network optimization, together with dedicated design strategies tailored to each setting. While these baselines already reveal useful design principles and enable scalable optimization, they are not the end of the story. Rather, they provide a foundation for more practical and sophisticated pinching-antenna deployments, where richer propagation effects, dynamic environment effects, and diverse application requirements must be jointly accounted for. Moving forward, promising directions include extensions to time-varying environments and fast reconfiguration, robust design under traffic/blockage uncertainty, large-scale multi-waveguide deployments with coordination constraints, and multi-functional pinching antenna configurations supporting heterogeneous services (e.g., communication, localization, and sensing).

VI. SIMULATION RESULTS

In this section, numerical results are presented to validate the performance of the proposed algorithms for geometry-aware pinching-antenna system designs. Unless otherwise stated, the main simulation parameters are summarized in Table II. For the geometry-aware evaluation, users are assumed to be uniformly distributed over the communication region. All performance metrics are computed as spatial averages over a uniform $N_h \times N_v$ grid, after excluding the grid points that

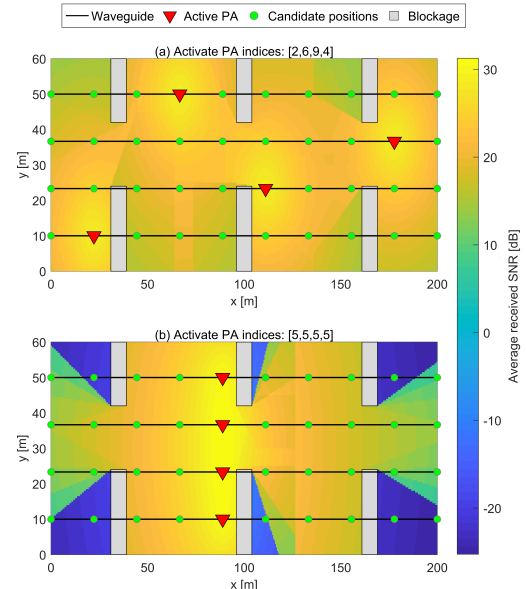


Fig. 2: Top-view of the considered three-dimensional geometry-aware environment with average received SNR maps for two representative pinching-antenna deployments.

fall inside the obstacle footprints. The environment contains $K = 6$ rectangular cuboid obstacles with height $H_{blk} < d_v$. A direct link between a pinching antenna at height d_v and a floor user is declared blocked if the corresponding three-dimensional line segment intersects the volume of any obstacle. Unless otherwise specified, the obstacles are placed as follows:

$$\mathcal{B}(x_c, y_1, y_2) \triangleq [x_c - \frac{w}{2}, x_c + \frac{w}{2}] \times [y_1, y_2] \times [0, H_{blk}], \quad (36)$$

where $x_c \in \{14, 40, 66\}$, $w = 8 \text{ m}$ and $(y_1, y_2) \in \{(0, 20), (35, 50)\} \text{ m}$.

For a better illustration, we present the top-view of the considered geometry-aware scenario in Fig. 2. Fig. 2 shows two examples of the resulting average received SNR maps under different pinching-antenna deployments, where Fig. 2(a) corresponds to the active pinching antenna indices [2, 6, 9, 4] (i.e., a more spatially distributed activation along the wave-

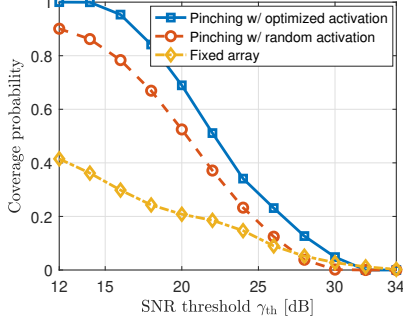


Fig. 3: Average-SNR-threshold coverage probability versus the SNR threshold γ_{th} with $N = 4$ and $M = 10$.

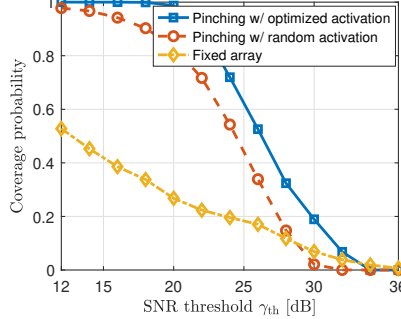


Fig. 4: Average-SNR-threshold coverage probability versus the SNR threshold γ_{th} with $N = 8$ and $M = 20$.

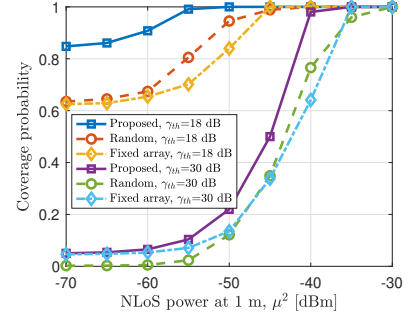


Fig. 5: Sensitivity of the average-SNR-threshold coverage probability to the NLoS power parameter μ^2 .

uides), while Fig. 2(b) corresponds to $[5, 5, 5, 5]$ (i.e., a more aligned activation around a similar x -location). As seen, the distributed activation in Fig. 2(a) yields a more balanced SNR distribution across the region by providing diversity against distance loss and obstacle-induced LoS blockage. In contrast, the aligned activation in Fig. 2(b) results in pronounced low-SNR areas, especially near the edges and behind obstacles, since many user locations rely on blocked or long paths to the clustered active pinching antennas. This comparison further motivates geometry-aware deployment design, where exploiting spatial diversity is key to mitigating coverage “dead zones”.

Fig. 3 illustrates the average-SNR-threshold coverage probability as a function of the SNR threshold γ_{th} under a uniform user distribution. For each γ_{th} , the coverage probability is computed as the fraction of valid grid points whose average received SNR exceeds γ_{th} , where grid points inside obstacle footprints are excluded. Three schemes are compared, namely, pinching antennas with optimized activation obtained by the proposed algorithm, pinching antennas with random activation where one candidate position per waveguide is selected uniformly at random, and a fixed N -element antenna array placed at the center of the communication region, where the antenna elements are half-wavelength spaced and are placed at the same height as the waveguides.

As observed in Fig. 3, the proposed optimized activation scheme consistently achieves the highest coverage probability over most of the considered threshold range. This indicates that, by adaptively selecting the active pinching locations across waveguides, the proposed method can better exploit spatial degrees of freedom to increase the fraction of locations meeting a target SNR requirement, especially in the presence of obstacle-induced LoS blocking and distance-dependent path loss. Random activation provides intermediate performance and generally outperforms the fixed-array baseline at moderate thresholds, since the pinching architecture still offers spatial diversity even without optimization. In contrast, the fixed array exhibits a noticeably lower coverage level at small and moderate γ_{th} , reflecting the inherent limitation of a static, centrally located deployment in serving spatially distributed users under blockage.

It is also seen that, when γ_{th} becomes very large, the fixed array may slightly outperform the pinching-based schemes.

This behavior is expected because the fixed array concentrates all N antenna elements within a very small aperture around the region center, thereby creating a localized “hot spot” with exceptionally high received SNR in its near vicinity. Such a strong local peak can contribute non-negligibly to the coverage probability under extremely stringent thresholds. In comparison, the pinching antennas are constrained to select one active radiating point on each waveguide from a discrete candidate set, and the resulting radiated power is spatially distributed across different waveguides and locations; while this improves overall spatial coverage at practical thresholds, it may yield a slightly smaller area that exceeds a very high γ_{th} . As γ_{th} increases further, the coverage of all schemes eventually decreases toward zero, while the proposed scheme maintains a clear advantage over the two baselines over a wide operating range, highlighting the benefit of geometry-aware activation optimization for coverage enhancement.

Fig. 4 further evaluates the average-SNR-threshold coverage probability as a function of the SNR threshold γ_{th} for the case with $N = 8$ waveguides/pinching antennas and $M = 20$ candidate positions per waveguide. Compared with Fig. 3, which corresponds to $(N, M) = (4, 10)$, increasing the spatial degrees of freedom to $(8, 20)$ yields a clear upward shift of all coverage curves, with the improvement being most pronounced in the low-to-moderate SNR regime. This trend is expected because activating more pinching antennas provides stronger power aggregation and additional spatial diversity, while a denser candidate set offers finer location resolution, enabling the optimized activation to select radiating points that better align with favorable LoS corridors and mitigate obstacle-induced shadowing. Consequently, for moderate γ_{th} , a larger portion of the region can satisfy the SNR requirement, and the performance advantage of optimized activation becomes more evident. In contrast, when γ_{th} is very large, the coverage probability of all schemes remains small and becomes less sensitive to further increasing (N, M) . This is because the high-threshold regime is dominated by a few localized high-SNR “hot spots”, whose existence and spatial extent are mainly dictated by the strongest available LoS links and the minimum achievable path loss in the given geometry. Once such hot spots are formed, adding more antennas or candidate points has limited impact on expanding the area that exceeds an extremely stringent γ_{th} . As a result, although

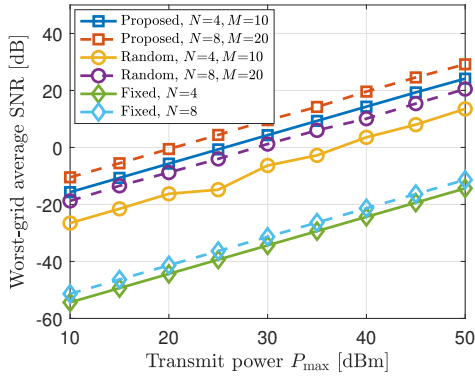


Fig. 6: Worst-grid average-SNR performance versus transmit power P_{\max} .

enlarging (N, M) yields only marginal improvement at high SNR thresholds, it significantly enhances the coverage in the practical SNR regime.

Fig. 5 evaluates the impact of the NLoS power level μ^2 on the average-SNR-threshold coverage probability for the geometry-aware scenario. Two representative SNR thresholds, $\gamma_{\text{th}} = 18$ dB and $\gamma_{\text{th}} = 30$ dB, are considered. Three schemes are compared, including pinching antennas with optimized activation obtained by the proposed algorithm, pinching antennas with random activation, and a fixed centered antenna-array baseline. As shown in Fig. 5, increasing μ^2 monotonically improves the coverage probability for all schemes, since a stronger NLoS component lifts the average received SNR even when LoS links are blocked. At the moderate threshold $\gamma_{\text{th}} = 18$ dB, the coverage is already high for the proposed scheme over a wide range of μ^2 , while the fixed-array and random-activation baselines exhibit a more visible dependence on μ^2 , indicating that the proposed optimized activation is less reliant on NLoS strength due to its ability to select favorable activation locations. In contrast, at the stringent threshold $\gamma_{\text{th}} = 30$ dB, the coverage is more sensitive to μ^2 and remains low when μ^2 is weak, because meeting such a high SNR requirement typically requires either strong LoS links or a sufficiently large NLoS power. As μ^2 increases, the performance gap between the proposed scheme and the two baselines is most pronounced in the intermediate regime, where NLoS is neither negligible nor dominant; in this regime, optimized activation can still exploit geometry to form higher-SNR regions, whereas random activation and the fixed array are less effective. When μ^2 becomes sufficiently large, the curves approach one and the differences diminish, since the SNR becomes increasingly dominated by the NLoS component and the benefit of geometry-aware activation is reduced.

Fig. 6 plots the achieved worst-grid average SNR as a function of the transmit power P_{\max} for the geometry-aware max-min average-SNR design. Here, the worst-grid average SNR is defined as the minimum, over all valid grids (excluding those inside the obstacle footprints), of the average received SNR. We compare three schemes, namely the proposed pinching-antenna design with optimized activation obtained by the proposed algorithm, pinching antennas with random activation, and a fixed centered N -element antenna array

with half-wavelength spacing deployed at the same height as the waveguides. To illustrate the impact of deployment freedom, the results are shown for two configurations, i.e., $(N, M) = (4, 10)$ and $(N, M) = (8, 20)$, where N denotes the number of waveguides/active pinching antennas and M denotes the number of candidate locations per waveguide.

As observed in Fig. 6, all schemes increase approximately linearly (in dB) with P_{\max} , as the average received SNR scales proportionally with transmit power under the adopted average-SNR model. More importantly, for both $(N, M) = (4, 10)$ and $(N, M) = (8, 20)$, the proposed optimized activation consistently achieves the largest worst-grid SNR across the entire power range, demonstrating that geometry-aware activation can effectively mitigate the most unfavorable locations caused by distance-dependent path loss and obstacle-induced LoS blocking. Random activation provides a noticeable improvement over the fixed-array baseline but remains clearly below the optimized design, indicating that while the pinching architecture offers inherent spatial diversity, explicit optimization is crucial for substantially lifting the worst-case performance. The fixed centered array yields the lowest worst-grid SNR, reflecting the limitation of a static deployment in a blockage-rich environment: the max-min objective is dominated by a small set of severely shadowed or farthest grids, and without the ability to relocate radiating points, the fixed array cannot eliminate these geometric “dead zones,” leading to a persistently low minimum SNR even when P_{\max} increases.

Comparing the two configurations in Fig. 6, increasing the spatial degrees of freedom from $(N, M) = (4, 10)$ to $(N, M) = (8, 20)$ yields a clear improvement for the pinching-antenna schemes, where the curves of both optimized activation and random activation are shifted upward by roughly ~ 10 dB over the considered power range. This gain is expected since more waveguides/active points provide stronger power aggregation and richer spatial diversity, while a denser candidate set enables finer-grained placement so that the activation can better target and alleviate the most unfavorable (worst-grid) locations created by distance-dependent attenuation and obstacle-induced shadowing. In contrast, the fixed-array baseline benefits much less from increasing N , exhibiting only a limited improvement. The reason is that the worst-grid metric is dominated by a few bottleneck grids that lie in deep shadow or far-field corners, and a centrally deployed fixed array cannot relocate its radiation points to mitigate these geometric dead zones. As a result, additional antennas mainly enhance already-strong directions but do not substantially raise the minimum SNR across the entire region. Overall, these results confirm that additional deployment freedom translates more effectively into worst-case performance gains for the pinching architecture, especially when combined with geometry-aware activation optimization.

Fig. 7 visualizes the optimized pinching-antenna deployments obtained for the two geometry-aware design problems in the same blockage environment. The background colormap shows the resulting spatial map of the average received SNR evaluated on a uniform grid after excluding the grid points that fall inside the blockage footprints. A single shared colorbar is

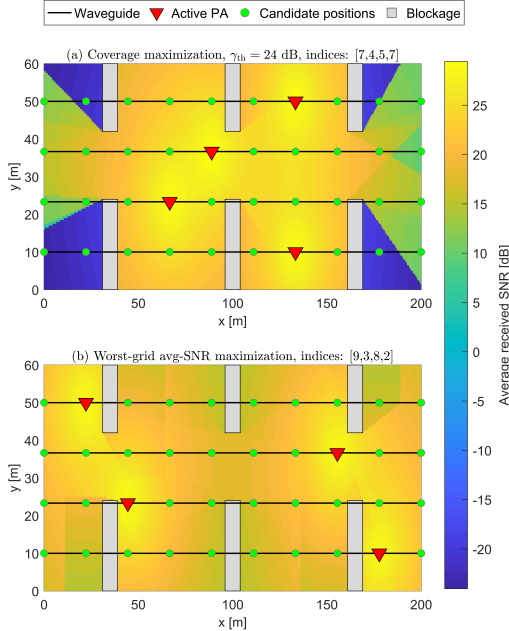


Fig. 7: Top-view of the considered geometry-aware environment with optimized pinching-antenna deployments for two representative design objectives: (a) average-SNR-threshold coverage maximization with $\gamma_{th} = 24$ dB; (b) worst-grid average-SNR maximization.

used for both subfigures to facilitate a direct visual comparison of the achieved SNR levels and the spatial patterns.

In Fig. 7(a), the deployment is optimized for the average-SNR-threshold coverage maximization with a target threshold $\gamma_{th} = 24$ dB, and the corresponding activated pinching antenna indices are [6, 5, 3, 6]. The selected pinching locations tend to create relatively strong SNR regions that cover a large portion of the feasible area, while accepting that some peripheral regions and obstacle-shadowed corners remain below the threshold. In contrast, Fig. 7(b) shows the deployment optimized for the worst-grid average-SNR maximization, with activated indices [2, 7, 4, 9]. Compared with (a), the activated points in (b) are more “spread out” across the waveguides and tend to shift toward locations that improve the weakest regions, leading to a more balanced SNR distribution with fewer pronounced low-SNR areas.

The different activation patterns in Fig. 7 directly reflect the distinct design philosophies of the two objectives. Coverage maximization is threshold-driven: it aims to maximize the fraction of grids whose SNR exceeds γ_{th} , and therefore it is beneficial to position some radiating points so as to enlarge high-SNR regions around favorable LoS corridors, even if this leaves a few highly shadowed or far-away grids unimproved. This behavior is visible in Fig. 7(a), where strong regions dominate much of the interior while the corners behind blockages still exhibit low SNR. On the other hand, worst-grid maximization is fairness-oriented: it is governed by the minimum SNR over all grids, and thus it forces the activation to explicitly mitigate “dead zones” by improving the most disadvantaged locations. Consequently, the optimized deployment in Fig. 7(b) tends to avoid concentrating radiating points on already-strong areas and instead reallocates degrees of freedom to lift the weakest parts of the region. Overall, Fig. 7 highlights

that, even under the same hardware constraints and blockage geometry, geometry-aware activation optimization can yield markedly different pinching antenna placements depending on whether the design goal prioritizes coverage at a target SNR level or worst-case spatial fairness.

VII. CONCLUSION

This paper investigated geometry-aware network-level design for generalized pinching-antenna systems in blockage-rich environments. By discretizing the service region into grids and modeling the environment with three-dimensional cuboid obstacles, we introduced a deterministic LoS visibility indicator to capture geometry-induced LoS/NLoS transitions between candidate pinching-antenna locations and grid points. Under a practical discrete activation model, we derived tractable per-grid average-SNR expressions whose geometry-dependent components can be precomputed offline, enabling an efficient offline–online optimization workflow. Building on these metrics, we formulated two geometry-aware network-level optimization problems: average-SNR-threshold coverage maximization and fairness-oriented worst-grid average-SNR maximization. Efficient solution methods were developed, including a low-complexity coordinate-ascent algorithm for the coverage maximization, and an epigraph-based bisection framework with efficient feasibility checks for the worst-grid average SNR maximization. Numerical results demonstrated that geometry-aware pinching-antenna activation can improve both coverage probability and worst-grid SNR over representative fixed-array and random-activation baselines, while also revealing how the coverage–robustness tradeoff evolves with blockage layouts and key system parameters. Future work may extend the proposed framework to multi-cell deployments, and imperfect or dynamically learned environment maps, as well as to hybrid traffic-and-geometry-aware objectives that better reflect time-varying network operations.

APPENDIX A PROOF OF LEMMA 1

For grid $(u, v) \in \Omega$, let $\Gamma(\psi_{u,v}; \mathbf{A})$ denote the instantaneous SNR under activation \mathbf{A} as defined in (17). The corresponding per-grid average received SNR is defined as

$$\bar{\Gamma}(\psi_{u,v}; \mathbf{A}) \triangleq \mathbb{E}[\Gamma(\psi_{u,v}; \mathbf{A})] = \rho \mathbb{E}\left[\|\tilde{h}(\psi_{u,v}; \mathbf{A})\|^2\right], \quad (37)$$

where $\rho \triangleq P/\sigma^2$ and the expectation is taken over the small-scale fading.

Using (13)–(14) and $\sum_{m=1}^M a_{n,m} = 1$, we obtain

$$\mathbb{E}\left[\|\tilde{h}(\psi_{u,v}; \mathbf{A})\|^2\right] = \sum_{n=1}^N \sum_{m=1}^M a_{n,m} \bar{G}_{n,m}(\psi_{u,v}), \quad (38)$$

where

$$\bar{G}_{n,m}(\psi_{u,v}) \triangleq \mathbb{E}\left[|h_{n,m}(\psi_{u,v})|^2\right] \quad (39)$$

denotes the average channel power from candidate (n, m) to grid (u, v) . Recalling (9) and noting that $h_{n,m}^{\text{NLoS}}(\psi_{u,v})$ is zero-mean and independent of the deterministic LoS term, we have

$$\bar{G}_{n,m}(\psi_{u,v}) = \chi_{n,m}(\psi_{u,v}) |h_{n,m}^{\text{LoS}}(\psi_{u,v})|^2$$

$$+ \mathbb{E} \left[|h_{n,m}^{\text{NLoS}}(\psi_{u,v})|^2 \right]. \quad (40)$$

From (10), we have

$$|h_{n,m}^{\text{LoS}}(\psi_{u,v})|^2 = \frac{\eta}{r_{n,m}^2(\psi_{u,v})}. \quad (41)$$

Moreover, with (12), the average NLoS power is given by

$$\mathbb{E} \left[|h_{n,m}^{\text{NLoS}}(\psi_{u,v})|^2 \right] = \sum_{\ell=1}^{N_c} \frac{\mu_{\ell}^2}{r_{n,m}^2(\psi_{u,v})} = \frac{\mu^2}{r_{n,m}^2(\psi_{u,v})}, \quad (42)$$

where $\mu^2 \triangleq \sum_{\ell=1}^{N_c} \mu_{\ell}^2$ denotes the aggregated NLoS channel power. Therefore, we have

$$\bar{G}_{n,m}(\psi_{u,v}) = \frac{\chi_{n,m}(\psi_{u,v}) \eta + \mu^2}{r_{n,m}^2(\psi_{u,v})}. \quad (43)$$

Substituting (38) and (43) into (37) yields (18). This completes the proof. \blacksquare

APPENDIX B PROOF OF PROPOSITION 1

We prove NP-hardness by a polynomial-time reduction from the *Maximum Coverage* (MC) problem, which is NP-hard [32]. To this end, let us first present the definition of the MC problem. Given a universe $\mathcal{U} = \{1, \dots, G\}$ and a collection of subsets $\{\mathcal{S}_j\}_{j=1}^J$ with $\mathcal{S}_j \subseteq \mathcal{U}$, together with an integer budget k , the MC problem is given by²

$$\max_{\mathcal{J} \subseteq \{1, \dots, J\}, |\mathcal{J}|=k} \left| \bigcup_{j \in \mathcal{J}} \mathcal{S}_j \right|. \quad (44)$$

As seen, the MC problem aims to select a subcollection \mathcal{J} with $|\mathcal{J}| \leq k$ so that the union $\bigcup_{j \in \mathcal{J}} \mathcal{S}_j$ covers as many distinct elements in \mathcal{U} as possible.

Recall that to prove NP-hardness of (23), it suffices to show that a known NP-hard problem reduces to (23) in polynomial time, i.e., $\text{MC} \leq_p (23)$ [33]. Here, we write $A \leq_p B$ if there exists a polynomial-time computable mapping f from instances of A to instances of B such that the answer to an instance x of A can be obtained from the answer to $f(x)$ of B in polynomial time. Next, we show how to map any MC instance $(\mathcal{U}, \{\mathcal{S}_j\}_{j=1}^J, k)$ to a special instance of (23) in polynomial time. Given any MC instance $(\mathcal{U}, \{\mathcal{S}_j\}_{j=1}^J, k)$, we construct a special instance of (23) such that (i) each waveguide activates exactly one candidate (as in our model), yet (ii) the number of distinct candidates effectively selected is at most k , matching the MC budget. Moreover, a grid is “covered” in MC if and only if its average SNR reaches the threshold in (23). The construction is as follows.

- *Grids \leftrightarrow MC elements:* Let the grid index set Ω contain $|\Omega| = G$ grids, in one-to-one correspondence with the elements in \mathcal{U} . Throughout, “grid i ” represents element $i \in \mathcal{U}$.
- *Budget \leftrightarrow number of waveguides:* Set the number of waveguides to $N = k$.

²The standard MC problem uses the constraint $|\mathcal{J}| \leq k$. For technical convenience, we consider the exact- k variant, i.e., $|\mathcal{J}| = k$, which is also NP-hard. This choice will simplify the subsequent reduction by aligning with the “one active pinching antenna per waveguide” structure in our setting.

- *Candidates \leftrightarrow MC sets:* On each waveguide $n \in \{1, \dots, N\}$, set the number of candidate positions to $M = J$. Candidate $m \in \{1, \dots, J\}$ corresponds to the MC set \mathcal{S}_m .

- *Encoding set membership via SNR contributions:* Let $\gamma_{\text{th}} > 0$ be the SNR threshold in (23). Define the (precomputable) per-grid average-SNR contribution of candidate (n, m) to grid $i \in \Omega$ as³

$$\bar{\Gamma}_{n,m}(i) \triangleq \begin{cases} \gamma_{\text{th}}, & \text{if } i \in \mathcal{S}_m, m \in \{1, \dots, J\}, \\ 0, & \text{otherwise,} \end{cases} \quad (45)$$

so that activating candidate $m \in \{1, \dots, J\}$ contributes exactly γ_{th} to precisely those grids whose indices belong to \mathcal{S}_m , and contributes 0 otherwise. Then, under an activation matrix $\mathbf{A} = [a_{n,m}]$, define the per-grid average SNR as

$$\bar{\Gamma}(i; \mathbf{A}) \triangleq \sum_{n=1}^N \sum_{m=1}^M a_{n,m} \bar{\Gamma}_{n,m}(i), \quad \forall i \in \Omega. \quad (46)$$

The above construction is computable in time polynomial in (G, J, k) . Then, with (46), the MILP (23) reduces to

$$\max_{\mathbf{A}, \{c_i\}} \sum_{i \in \Omega} c_i \quad (47a)$$

$$\text{s.t. } \bar{\Gamma}(i; \mathbf{A}) \geq \gamma_{\text{th}} c_i, \quad \forall i \in \Omega, \quad (47b)$$

$$\sum_{m=1}^M a_{n,m} = 1, \quad \forall n = 1, \dots, N, \quad (47c)$$

$$a_{n,m} \in \{0, 1\}, \quad \forall n, m, \quad (47d)$$

$$c_i \in \{0, 1\}, \quad \forall i \in \Omega. \quad (47e)$$

Let OPT_{MC} and OPT_{MILP} denote the optimal objective values of (44) and (47), respectively. We show that $\text{OPT}_{\text{MILP}} = \text{OPT}_{\text{MC}}$.

(i) *Any MC solution induces a feasible MILP solution with the same objective.* Take any $\mathcal{J} \subseteq \{1, \dots, J\}$ with $|\mathcal{J}| = k$. Construct \mathbf{A} by assigning the k selected set indices in \mathcal{J} to the $N = k$ waveguides, i.e., for each $n \in \{1, \dots, k\}$ choose one distinct $j_n \in \mathcal{J}$ and set $a_{n,j_n} = 1$ (and $a_{n,m} = 0$ for $m \neq j_n$), so that (47c)–(47d) hold. Define

$$c_i \triangleq \mathbb{1} \left\{ i \in \bigcup_{j \in \mathcal{J}} \mathcal{S}_j \right\}, \quad \forall i \in \Omega. \quad (48)$$

If $c_i = 1$, then there exists $j \in \mathcal{J}$ such that $i \in \mathcal{S}_j$. By (45) and (46), at least one selected term equals γ_{th} , hence $\bar{\Gamma}(i; \mathbf{A}) \geq \gamma_{\text{th}}$ and (47b) holds. If $c_i = 0$, then (47b) holds trivially since $\bar{\Gamma}(i; \mathbf{A}) \geq 0$. Therefore, $(\mathbf{A}, \{c_i\})$ is feasible for (47), and its objective value is

$$\sum_{i \in \Omega} c_i = \left| \bigcup_{j \in \mathcal{J}} \mathcal{S}_j \right|. \quad (49)$$

Maximizing over all feasible \mathcal{J} yields $\text{OPT}_{\text{MILP}} \geq \text{OPT}_{\text{MC}}$.

(ii) *Any feasible MILP solution induces an MC solution with no smaller objective.* Conversely, take any feasible $(\mathbf{A}, \{c_i\})$

³We note that $\bar{\Gamma}_{n,m}(i)$ is *artificially defined* in the reduction (not derived from a physical channel model) to encode the set-membership relation $i \in \mathcal{S}_m$ via the threshold γ_{th} .

of (47). By (47c)–(47d), each waveguide selects exactly one candidate. Let $\mathcal{J}(\mathbf{A}) \subseteq \{1, \dots, J\}$ denote the set of indices selected by at least one waveguide under \mathbf{A} . Since there are $N = k$ waveguides, we have $|\mathcal{J}(\mathbf{A})| \leq k$. If $|\mathcal{J}(\mathbf{A})| < k$, we can add arbitrary extra indices from $\{1, \dots, J\} \setminus \mathcal{J}(\mathbf{A})$ to obtain a set $\widehat{\mathcal{J}}(\mathbf{A})$ with $|\widehat{\mathcal{J}}(\mathbf{A})| = k$. Clearly, $\bigcup_{j \in \widehat{\mathcal{J}}(\mathbf{A})} \mathcal{S}_j \supseteq \bigcup_{j \in \mathcal{J}(\mathbf{A})} \mathcal{S}_j$, so $\widehat{\mathcal{J}}(\mathbf{A})$ is feasible for (44) and can only increase (or keep) the union size.

Now, consider any grid i with $c_i = 1$. Constraint (47b) implies $\bar{\Gamma}(i; \mathbf{A}) \geq \gamma_{\text{th}}$. By (46)–(45), this is possible only if there exists at least one selected candidate $m \in \mathcal{J}(\mathbf{A})$ such that $i \in \mathcal{S}_m$. Hence,

$$\{i \in \Omega : c_i = 1\} \subseteq \bigcup_{m \in \mathcal{J}(\mathbf{A})} \mathcal{S}_m \subseteq \bigcup_{j \in \widehat{\mathcal{J}}(\mathbf{A})} \mathcal{S}_j, \quad (50)$$

which yields

$$\sum_{i \in \Omega} c_i \leq \left| \bigcup_{j \in \widehat{\mathcal{J}}(\mathbf{A})} \mathcal{S}_j \right|. \quad (51)$$

Therefore, the MC solution $\widehat{\mathcal{J}}(\mathbf{A})$ achieves an objective value no smaller than the MILP objective. Taking the maximum over all MILP feasible solutions gives $\text{OPT}_{\text{MC}} \geq \text{OPT}_{\text{MILP}}$.

Finally, combining (i) and (ii), we obtain $\text{OPT}_{\text{MILP}} = \text{OPT}_{\text{MC}}$ for the constructed instance, and the construction and mappings are polynomial-time. Therefore, if (23) could be solved in polynomial time, then MC could also be solved in polynomial time. Since MC is NP-hard, (23) is NP-hard (even restricted to instances of the form (47)), and hence (23) is NP-hard in general. This completes the proof. ■

REFERENCES

- [1] Z. Niu, "TANGO: traffic-aware network planning and green operation," *IEEE Wireless Commun.*, vol. 18, no. 5, pp. 25–29, Oct. 2011.
- [2] S. Bi, J. Lyu, Z. Ding, and R. Zhang, "Engineering radio maps for wireless resource management," *IEEE Wireless Commun.*, vol. 26, no. 2, pp. 133–141, Apr. 2019.
- [3] B. Partov, D. J. Leith, and R. Razavi, "Utility fair optimization of antenna tilt angles in LTE networks," *IEEE/ACM Trans. Networking*, vol. 23, no. 1, pp. 175–185, Feb 2015.
- [4] V. Buenestado, M. Toril, S. Luna-Ramírez, J. M. Ruiz-Avilés, and A. Mendo, "Self-tuning of remote electrical tilts based on call traces for coverage and capacity optimization in lte," *IEEE Trans. Veh. Technol.*, vol. 66, no. 5, pp. 4315–4326, May 2017.
- [5] Z.-Q. Luo, X. Zheng, D. López-Pérez, Q. Yan, X. Chen, N. Wang, Q. Shi, T.-H. Chang, and A. García-Rodríguez, "SRCON: A data-driven network performance simulator for real-world wireless networks," *IEEE Commun. Mag.*, vol. 61, no. 6, pp. 96–102, Jun. 2023.
- [6] Y. Zeng, J. Chen, J. Xu, D. Wu, X. Xu, S. Jin, X. Gao, D. Gesbert, S. Cui, and R. Zhang, "A tutorial on environment-aware communications via channel knowledge map for 6G," *IEEE Commun. Surv. Tutorials*, vol. 26, no. 3, pp. 1478–1519, thirdquarter 2024.
- [7] L. Li, Y. Xu, Y. Xue, F. Yin, C. Shen, R. Zhang, and T.-H. Chang, "PEMNet: Towards autonomous and enhanced environment-aware mobile networks," *IEEE Commun. Mag. (submitted)*, 2026, available online: arXiv:2601.11025.
- [8] B. Peng, S. Zhang, X. Zheng, Y. Xue, X. Qin, and T.-H. Chang, "RF-LSCM: Pushing radiance fields to multi-domain localized statistical channel modeling for cellular network optimization," 2025, arXiv preprint arXiv:2509.13686.
- [9] Y. Xu, J. Cui, Y. Zhu, Z. Ding, T.-H. Chang, R. Schober, V. W. Wong, O. A. Dobre, G. K. Karagiannidis, H. V. Poor, and X. You, "Generalized pinching-antenna systems: A tutorial on principles, design strategies, and future directions," *IEEE Commun. Surv. Tutorials (submitted)*, 2025, Available online: arXiv:2510.14166.
- [10] Z. Ding, R. Schober, and H. V. Poor, "Flexible-antenna systems: A pinching-antenna perspective," *IEEE Trans. Commun.*, vol. 73, no. 10, pp. 9236–9253, 2025.
- [11] K. Wang, Z. Ding, and L. Hanzo, "Generalized pinching-antenna systems: A leaky-coaxial-cable perspective," 2025, Available online: arXiv:2510.14166.
- [12] Y. Xu, Z. Ding, and G. K. Karagiannidis, "Rate maximization for downlink pinching-antenna systems," *IEEE Wireless Commun. Lett.*, vol. 14, no. 5, pp. 1431–1435, May 2025.
- [13] S. A. Tegos, P. D. Diamantoulakis, Z. Ding, and G. K. Karagiannidis, "Minimum data rate maximization for uplink pinching-antenna systems," *IEEE Wireless Commun. Lett.*, vol. 14, no. 5, pp. 1516–1520, 2025.
- [14] M. Zeng, X. Li, J. Wang, G. Huang, O. A. Dobre, and Z. Ding, "Energy-efficient resource allocation for NOMA-assisted uplink pinching-antenna systems," 2025, arXiv preprint arXiv:2505.07555.
- [15] G. Zhu, X. Mu, L. Guo, S. Xu, Y. Liu, and N. Al-Dahir, "SEE tradeoff in pinching-antenna systems: Waveguide multiplexing or waveguide switching?" 2026, available online: arXiv:2601.04844.
- [16] D. Tyrovolas, S. A. Tegos, P. D. Diamantoulakis, S. Ioannidis *et al.*, "Performance analysis of pinching-antenna systems," *IEEE Trans. Cognit. Commun. Networking*, pp. 1–1, 2025.
- [17] Y. Cheng, C. Ouyang, Y. Liu, and G. K. Karagiannidis, "On the performance of pinching-antenna systems (PASS) with orthogonal and non-orthogonal multiple access," 2025, available online: arXiv:2506.02420.
- [18] Z. Ding and H. V. Poor, "LoS blockage in pinching-antenna systems: Curse or blessing?" *IEEE Wireless Commun. Lett.*, pp. 1–1, 2025.
- [19] K. Wang, C. Ouyang, Y. Liu, and Z. Ding, "Pinching-antenna systems with LoS blockages," *IEEE Wireless Commun. Lett.*, vol. 14, no. 12, pp. 4122–4126, Dec. 2025.
- [20] L. Li, Y. Xu, T. Cai, and T.-H. Chang, "Power minimization in pinching-antenna systems under probabilistic LoS blockage," 2025, available online: arXiv:2512.24573.
- [21] R. Zhao, S. Hu, D. Mishra, and D. W. K. Ng, "Robust and secure blockage-aware pinching antenna-assisted wireless communication," 2026, available online: arXiv:2601.06430.
- [22] Y. Sun, Z. Ding, and G. K. Karagiannidis, "A stochastic geometric analysis on multi-cell pinching-antenna systems under blockage effect," *IEEE Wireless Commun. Lett.*, vol. 15, pp. 1085–1089, 2026.
- [23] R. Jiang, R. Zhang, Y. Xu, H. Hu, Y. Lu, and D. Niyato, "Spatially adaptive SWIPT with pinching antenna under probabilistic LoS blockage," 2025, available online: arXiv:2509.03038.
- [24] H. Hu, R. Jiang, Y. Xu, J. Ma, and F. Fang, "Average AoI in pinching antenna-assisted WPCNs with probabilistic LoS blockage," 2025, available online: arXiv:2511.05947.
- [25] Y. Xu, Y. Lu, Z. Ding, and T.-H. Chang, "Pinching-antenna system design under random LoS and NLoS channels," *IEEE Trans. Wireless Commun. (submitted)*, 2025, available online: arXiv:2512.04719.
- [26] Y. Xu, Z. Ding, O. A. Dobre, and T.-H. Chang, "Pinching-antenna system design with LoS blockage: Does in-waveguide attenuation matter?" *IEEE Trans. Wireless Commun. (submitted)*, 2025, available online: arXiv:2508.07131.
- [27] X. Xie, F. Fang, Z. Ding, and X. Wang, "Pinching antennas in blockage-aware environments: Modeling, design, and optimization," 2026, available online: arXiv:2601.01277.
- [28] Z. Ding, R. Schober, and H. V. Poor, "Environment division multiple access (EDMA): A feasibility study via pinching antennas," 2025, available online: arXiv:2511.03820.
- [29] 3GPP, "Study on channel model for frequencies from 0.5 to 100 GHz," 3GPP TR 38.901 version 16.1.0 Release 16, Tech. Rep., 2020.
- [30] Y. Xu, Z. Ding, R. Schober, and T.-H. Chang, "Pinching-antenna systems with in-waveguide attenuation: Performance analysis and algorithm design," *IEEE Trans. Wireless Commun. (submitted)*, 2025, available online: arXiv:2506.23966.
- [31] L. A. Wolsey and G. L. Nemhauser, *Integer and Combinatorial Optimization*. John Wiley & Sons, 1999.
- [32] S. Khuller, A. Moss, and J. S. Naor, "The budgeted maximum coverage problem," *Inf. Process. Lett.*, vol. 70, no. 1, pp. 39–45, 1999.
- [33] S. Arora and B. Barak, *Computational Complexity: A Modern Approach*. Cambridge University Press, 2009.